Article

Structure of Ternary Imide LiCa(NH) and Hydrogen Storage Mechanisms in Amide#Hydride System

Hui Wu

J. Am. Chem. Soc., **2008**, 130 (20), 6515-6522 • DOI: 10.1021/ja800300e • Publication Date (Web): 30 April 2008

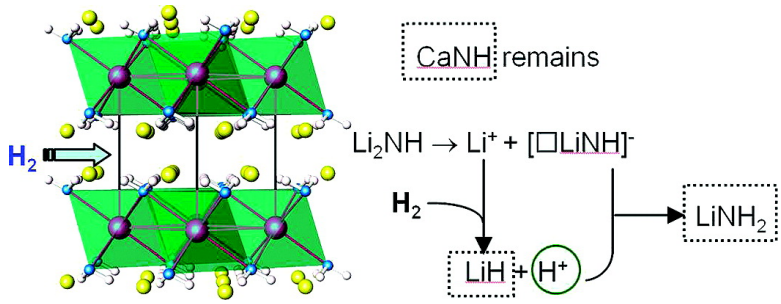

More About This Article

Additional resources and features associated with this article are available within the HTML version:

- Supporting Information
- Links to the 2 articles that cite this article, as of the time of this article download
- Access to high resolution figures
- Links to articles and content related to this article
- Copyright permission to reproduce figures and/or text from this article

View the Full Text HTML

Journal of the American Chemical Society is published by the American Chemical Society. 1155 Sixteenth Street N.W., Washington, DC 20036

J|A|C|S
ARTICLES

Published on Web 04/30/2008

Structure of Ternary Imide $Li_2Ca(NH)_2$ and Hydrogen Storage Mechanisms in Amide−Hydride System

Hui Wu

NIST Center for Neutron Research, National Institute of Standards and Technology, 100 Bureau Drive, MS 8562, Gaithersburg, Maryland 20899-6102, and Department of Materials Science and Engineering, University of Maryland College Park, Maryland 20742-2115

Received January 14, 2008; E-mail: huiwu@nist.gov

Abstract: The crystal structure of the ternary imide $Li_2Ca(NH)_2$ has been determined using neutron powder diffraction data on a deuterated sample. The structure consists of infinite layers of edge-shared $Ca[NH]_6$ octahedra, which are separated by Li cations. The mobile Li^+ ions in such two-dimensional channels defined by $Ca[NH]_6$ octahedra layers are shown to have a great impact on the hydrogenation properties of the imide. Through detailed structural analysis on the products at various stages of desorption and absorption of the amide−hydride mixture, we proposed a dehydrogenation mechanism involving the mobile small ions in both amide and hydride and a hydrogen storage mechanism for the ternary imide.

1. Introduction

Lithium nitride/imide, with a hydrogen storage potential up to 10.4 wt %, has been viewed as a promising hydrogen storage system.[1] The hydrogenation of lithium nitride involves a two-step reaction and can be written as

$$Li_3N + 2H_2 \overset{a}{\leftrightarrow} Li_2NHLiH + H_2 \overset{b}{\leftrightarrow} LiNH_2 + 2LiH \quad (1)$$

However, its practical application for hydrogen storage is limited because of the low hydrogen pressure (<0.01 bar) and the high desorption temperature (T_{des} > 320 °C) of reaction 1a, and thus the reversible capacity of the system (reaction 1b) is reduced to only 5.2 wt %.

Other factors, such as mixing conditions (close proximity),[2] the presence of catalysis,[3] initial precursor mixing ratios,[4] purity of the precursors,[5] particle size,[2,3,6] and different gases present,[3,5] make it difficult to establish a direct and unambiguous hydrogenation/dehydrogenation mechanism within the system and to discern an effective approach to improve its storage performance.

Another feature of this system that complicates the decomposition mechanism is the competing release of ammonia from $LiNH_2$ at high temperature. A prior study of the decomposition kinetics of $LiNH_2$ noticed the presence of nonstoichimetric imide within a homogeneity range between $LiNH_2$ and Li_2NH.[5] Recently, high-resolution synchrotron X-ray diffraction was utilized to study the changes in the structure of $LiNH_2/Li_2NH$ during dehydrogenation and hydrogenation. The resolution of these experiments revealed new details of the nonstoichiometry within $Li_2NH/LiNH_2$ system.[2] In addition to confirming the formation of nonstoichiometric imides, David et al. proposed an ammonia-mediated mechanism associated with migration of lithium ions for hydrogen storage. The presence of Frenkel defect pairs in lithium imide was suggested to be the key in the decomposition process of $LiNH_2$ and the resultant production of ammonia.[2]

To reduce the desorption/absorption temperatures (T_{des}/T_{abs}) of pure lithium amide/imide, in addition to the use of catalysts and reduced particle size, several investigations have been conducted on the effects of hydride additives (LiH, MgH_2, CaH_2) on the T_{des}/T_{abs} and the amount of ammonia released in these systems.[3,7−11] In some cases, it has been claimed that the T_{des}/T_{abs} of the mixed amide/hydride systems can be significantly reduced compared to the results for pure $LiNH_2$. For systems with certain ratios of amide and hydride, the ammonia produced was also minimized. However, the hydrogen storage and release mechanism of these amide/hydride mixed systems was not established mainly due to the lack of accurate crystallographic information on the ternary imides formed after dehydrogenation. It has been proposed therefore that the ternary imides are directly formed via the interactions between amide and hydride.[9]

Although structures of binary imides have been studied for decades, problems still exist in determining their possible polymorphs at various temperatures and pressures.[12] Compared to the well-known binary imides, ternary imides with mixed alkali and alkaline earth cations have not attracted attention until

(1) Chen, P.; Xiong, Z.; Luo, J.; Lin, J.; Tan, K. L. *Nature* **2002**, *420*, 302–304.
(2) David, W. I. F.; Jones, M. O.; Gregory, D. H.; Jewell, C. M.; Johnson, S. R.; Walton, A.; Edwards, P. P. *J. Am. Chem. Soc.* **2007**, *129*, 1594–1601.
(3) Ichikawa, T.; Hanada, H.; Isobe, S.; Leng, H.; Fujii, H. *J. Phys. Chem. B* **2004**, *108*, 7887–7892.
(4) Chen, P.; Xiong, Z.; Luo, J.; Lin, J.; Tan, K. L. *J. Phys. Chem. B* **2003**, *107*, 10967–10970.
(5) Pinkerton, F. E. *J. Alloys Compd.* **2005**, *400*, 76–82.
(6) Hu, Y. H.; Ruckenstein, E. *J. Phys. Chem. A* **2003**, *107*, 9737–9739.
(7) Luo, W. *J. Alloys Compd.* **2004**, *381*, 284–287.
(8) Luo, W.; Sickafoose, S. *J. Alloys Compd.* **2006**, *407*, 274–281.
(9) Xiong, Z. T.; Wu, G. T.; Hu, J. J.; Chen, P. *Adv. Mater.* **2004**, *16*, 1522–1525.
(10) Tokoyoda, K.; Hino, S.; Ichikawa, T.; Okamoto, K.; Fujii, H. *J. Alloys Compd.* **2007**, *439*, 337–341.
(11) Orimo, S.; Nakamori, Y.; Eliseo, J. R.; Züttel, A.; Jensen, C. M. *Chem. Rev.* **2007**, *107*, 4111–4132.
(12) Balogh, M.; Jones, C. Y.; Herbst, J. F., Jr.; Kundrat, M. *J. Alloys Compd.* **2006**, *420*, 326–336.

recently, when they were discovered during dehydriding the mixed amide and hydride systems.[8,9] A recent study using combined synchrotron X-ray and neutron powder diffraction (NPD) techniques revealed the detailed structure of $Li_2Mg(NH)_2$, indicating the existence of cation vacancies in its three polymorphs.[13] The detailed structure of $Li_2Ca(NH)_2$ is still unclear owing to the lack of NPD data on the deuterated samples.[10,14] Therefore, the mechanism of rehydrogenation of these ternary imides remains uncertain. It seems clear that the structures of these ternary imides hold the key to revealing the dehydrogenation/rehydrogenation process in the mixed amide and hydride systems.

The work presented here focuses on the $LiNH_2-CaH_2$ system. First, we have determined the crystal structure of ternary imide $Li_2Ca(ND)_2$ by high-resolution NPD. And then we examined the products produced at various stages of desorption from the mixture of $2LiNH_2 + CaH_2$ by X-ray diffraction. Our results suggest an alternative mechanism for dehydrogenation reactions in the mixed amide/hydride systems and a hydrogen storage mechanism for the ternary imides. This finding holds the key to understanding the mechanism for dehydrogenation and the rehydrogenation in the mixed amide and hydride systems and is critical for rational development of a better candidate system for hydrogen storage.

2. Experimental Details

Samples of $Li_2Ca(NH)_2$ were synthesized by mixing the stoichiometric ratios (2:1) of $LiNH_2$ (95%, Aldrich) and CaH_2 (99.9%, Aldrich) powders via ball milling with a Fritsch Pulverisette 7 planetary mill at 400 rpm for 60 min. The mixed product was then wrapped in Mo foil and loaded in a stainless steel tube. The tube was connected to a gas-flow system and heated in a tube furnace. The powder mixture was heated with a ramp of 1 K/min to 593 K and annealed at 593 K overnight under a constant Ar gas flow. Products at various desorption stages were monitored by interrupting the above heat treatment at certain points, which was detailed in the Results and Discussion section. $Li_2Ca(ND)_2$ sample for NPD study were prepared using the same procedure. Stoichiometric quantities (2:1 ratio) of the $LiND_2$ and CaD_2 were mixed with an agate mortar and a pestle. $LiND_2$ was prepared by the direct reaction from lithium nitride Li_3N (Aldrich) and deuterated ammonia (99.99%) at 623 K. CaD_2 was prepared by the reaction of Ca metal (Alfa Aesar 99.98%) with D_2 (99.999%) at 773 K. All sample handling was performed in a He-filled glovebox due to the extreme air-sensitivity of the hydrides.

Phase identification and equilibrium were first monitored on hydride samples sealed in glass capillaries using a Rigaku X-ray diffractometer with a Cu Kα source operated at 40 kV and 40 mA. The X-ray diffraction (XRD) pattern obtained on the samples using apreviously reported synthesis method[14] shows reflections from Li_2NH, CaH_2, $LiNH_2$, and CaNH, which indicates an incomplete dehydrogenation. Extended annealing after the simple heating ramp under Ar gas flow was required to obtain the single-phase target imide (majority phase >95 wt%). Dehydrogenation and the gaseous products were analyzed using Quantachrome Autosorb-1 equipped with a Quadrupde Mass Spectrometer (QMS).

Neutron powder diffraction (NPD) data were collected at the NIST Center for Neutron Research (NCNR, Gaithersburg, MD, USA) using the BT-1 high-resolution neutron powder diffractometer with the Cu(311) monochromator at $\lambda = 1.5403(2)$ Å. The powder samples were sealed into 3 mm diameter vanadium cans under an ultrapure He atmosphere. Data were collected over 15 h at 15 K and 295 K, respectively, in the 2θ range 3°–168° with a step size of 0.05°. Rietveld structural refinements were done using the GSAS package.[15] The hydrogen-to-metal ratios in the hydride samples were checked using the neutron prompt-γ activation analysis (PGAA) facility, which is able to detect hydrogen as low as 2 μg.[16] Pure LiH and CaH_2 samples were used as standards to normalize γ-ray intensities. Disk sample configuration was used for Li-containing hydride samples to decrease the amount of the neutrons absorbed by Li. The stoichiometry of H was found to be approximately Li/Ca/H ≈ 2.07:1:2.02 ("$Li_2CaN_2H_2$") in the completely dehydrogenated samples. The stoichiometry of H in the product after rehydrogenation is Li/Ca/H ≈ 2.02:1: 4.01 ("$Li_2CaN_2H_{4.01}$").

3. Results and Discussion

3.1. Structure Determination and Crystal Chemistry. The NPD pattern of $Li_2Ca(ND)_2$ could be indexed using a trigonal $P\bar{3}m1$ cell. A test refinement only considering lattice parameters and space group (LeBail refinement) could satisfactorily fit all peak profiles, confirming the right starting model. We then commenced the Rietveld refinement on the atomic coordinates with D atoms at various sites: (i) a model with D on 6*i* site and N−D pointing to the middle point of the two adjacent Li sites (see Figure S1 in the Supporting Information (SI)), as suggested by prior X-ray results and DFT calculations;[14] (ii) a model with D atoms equally distributed in the 12*f* site (12*f*-model), i.e., one N surrounded by six D sites in a 6-fold manner; (iii) a model with D equally on the 6*i* sites and N−D vectors toward the three adjacent Li atoms (6*i*-model). The refinement using the previously suggested model (i.e., model i) could not be well converged with good statistics and resulted in either an abnormally short N−D distance (0.439 Å) or a length (1.030 Å) even longer than those in $LiND_2$.[17] The D sites in the refined 12*f*-model also deviates considerably from the initial model; i.e., the initial six equally distributed D sites around one N were actually separated into three pairs, so that the 6-fold D distribution essentially became 3-fold with N−D pointing toward neighboring Li (see Figure S1 in the SI). These results strongly implied that D may distribute in the alternative 6*i* sites around each N atom (model iii: 6*i*-model). The refinement on the 6*i*-model yielded a better fit on the NPD pattern and did not result in significant deviation in the atomic positions and displacement parameters of Ca, Li. and N compared to the 12*f* -model. Details of structure determination and crystallographic parameters of these models are provided in the SI. The structural parameters of the refined 6*i*-model and 12*f*-model are listed in Table 1 and Table S2 (see SI). Other possibilities of hydrogen distribution were also considered (see SI). However, these models resulted in either diverged refinement or abnormal N−D bond distances with a very poor quality of fit. Also, no superstructure reflections were observed in the low temperature NPD pattern, which indicates no long-range order of D atoms in this ternary amide. Therefore, we believe the present 6*i*-model (3-fold D sites) with "partial disordering" of D (relative to the "complete disordering" in 12*f*-model) is the most likely structure for $Li_2Ca(NH)_2$ in the temperature range 15–295 K. A 3D Fourier difference map explicitly shows such 3-fold hydrogen sites in the lattice (see Figure S2). Of course, the 12*f*-model may become more favorable at higher temperature. The observed

(13) Rijssenbeek, J.; Gao, Y.; Hanson, J.; Huang, Q.; Jones, C.; Toby, B. *J. Alloys Compd.* **2008**, *454*, 233–244.
(14) Wu, G.; Xiong, Z.; Liu, T.; Liu, Y.; Hu, J.; Chen, P.; Feng, Y.; Wee, A. *Inorg. Chem.* **2007**, *46*, 517–521.
(15) Larson A. C.; Von Dreele, R. B. General Structure Analysis System, Report LAUR 86–748. Los Alamos National Laboratory, NM, 1994.
(16) Lindstrom, R. M. *J. Res. Natl. Inst. Stand. Technol.* **1993**, *98*, 127–133.
(17) Nagib, M.; Jacob, H. *Z. Anorg. Allg. Chem.* **1972**, *391*, 271.

Table 1. Refined Crystallographic Data for $Li_2Ca(ND)_2$: Space Group $P\bar{3}m1$ (No. 64)

atom	site	occupancy	*x*	*y*	*z*	U_{11}	U_{22}	U_{33}	U_{12}	U_{13}	U_{23}
15 K: $Li_2Ca(ND)_2$ model with D at 6*i*, a = 3.55894(9) Å, c = 5.9234(2) Å											
Ca	*1a*	1.00	0	0	0	0.8(1)	U_{11}	1.7(2)	0.44(4)	0	0
Li	*2d*	0.97(4)	0.3333	0.6667	0.6353(1)	2.3(3)	U_{11}	4.6(3)	1.1(1)	0	0
N	*2d*	1.00	0.3333	0.6667	0.2485(2)	1.20(4)	U_{11}	0.57(5)	0.60(2)	0	0
D	*6i*	0.34(1)	0.1007(2)	0.5503(1)	0.3205(1)	6.8(3)	7.2(3)	4.9(5)	3.4(1)	0.9(3)	0.4(1)
295 K: $Li_2Ca(ND)_2$ model with D at 6*i*, a = 3.56787(7) Å, c = 5.9482(2) Å											
Ca	*1a*	1.00	0	0	0	1.2(1)	U_{11}	1.7(2)	0.60(4)	0	0
Li	*2d*	0.86(3)	0.3333	0.6667	0.6370(1)	3.0(3)	U_{11}	3.5(4)	1.5(1)	0	0
N	*2d*	1.00	0.3333	0.6667	0.2495(2)	1.37(4)	U_{11}	0.82(6)	0.68(2)	0	0
D	*6i*	0.34(1)	0.0997(1)	0.5498(1)	0.3190(1)	6.9(3)	8.4(3)	6.2(5)	3.4(1)	1.8(2)	0.9(1)

and calculated NPD patterns using the present 6*i*-model are shown in Figure 1 and S3 (see SI). In addition, refinement on the Li site occupancy revealed the presence of Li cation vacancies, the amount of which significantly increases with temperature from 3% at 15 K to 14% at 295 K.

Figure 2 shows the crystal structure of $Li_2Ca(ND)_2$ with D randomly distributed on one of the three sites around each N atom. In this structure, each Ca is coordinated with six ND^{2-} anions, forming a nearly regular $Ca[ND]_6$ octahedron with six equal Ca−N bonds (2.527 Å) and an ∼90° N−Ca−N bond angle; each Li is bonded with four ND^{2-} anions with Li−N bond lengths in a range of 2.167–2.291 Å. Each ND^{2-} anion is surrounded by three Ca^{2+} and four Li^+, and its bond valence sum is $^2/_6 \times 3 + {}^1/_4 \times 4 = 2$, equal to its formal charge. Therefore, both cations and anions are completely bonded. Thus, $Li_2Ca(ND)_2$ is distinctly different from any of the polymorphs of $Li_2Mg(NH)_2$, which contain ordered or disordered cation vacancies and can be derived from Li_2NH with a formula of $[LiMg_{0.5}\square_{0.5}]NH$. $Li_2Ca(ND)_2$ cannot be viewed as the vacancy-containing derivative $[LiCa_{0.5}\square_{0.5}]NH$ from Li_2NH. Consequently, the hydrogen site should not be necessarily referred to that in the Li_2NH lattice as proposed previously.[14] Here, we want to point out that the 3–14% Li vacancy observed in $Li_2Ca(ND)_2$ according to our NPD refinement is associated with defect reactions at elevated temperatures (see discussion below). This is different from those in $[LiMg_{0.5}\square_{0.5}]NH$, where the cation vacancy is charge compensated by the Mg^{2+} substituent and can be treated as a structural component. Such a structural distinction between these two ternaries is not unexpected because the ionic radii of Li and Mg are nearly identical (0.59 Å vs 0.57 Å) while there is a significant size mismatch (0.59 Å vs 1.00 Å) and coordination preference (IV vs VI) between Li and Ca. In fact, the large difference in size and coordination preference is the driving force leading to an ordered arrangement of alternating $Ca[NH]_6$ octahedra and $Li[NH]_4$ tetrahedra along the *c*-axis in the present case. These octahedra and tetrahedra are the basic units in CaNH and Li_2NH, respectively, and in that sense $Li_2Ca(NH)_2$ can actually be viewed as a combined-imide structure consisting of two different imide layers (Figure 2).

We also note that $Li_2Ca(ND)_2$ possesses a structure similar to that of the oxide compound Li_2NiO_2 ($P\bar{3}m1$), if we treat the orientationally disordered NH^{2-} as O^{2-}. To rationalize such a comparison of structures and anions, it is useful to compare with other imide compounds. For example, Li_2NH and Li_2O both form the $Fm\bar{3}m$ antifluoride structure; CaNH is also isostructural with CaO ($Fm\bar{3}m$ rocksalt structure). Such structural analogues of NH^{2-} vs O^{2-} in imides and oxides are surprisingly very common in many alkali or alkaline earth imides. Therefore, $Li_2Ca(NH)_2$ can also be described as the layered structure consisting of infinite two-dimensional (2D) slabs of edge-shared $Ca[NH]_6$ octahedra, which are separated by the motif of Li cations (Figure 3a), as in many "Li-intercalated" layered oxides.

Given such a structural arrangement, we believe a likely explanation for the hydrogen positions and the orientation of N−H bonds should be related to the bonding between NH^{2-} and Ca^{2+} within the 2D slabs of $Ca[NH]_6$ octahedra. In the structure of $Li_2Ca(NH)_2$, although hydrogen atoms randomly

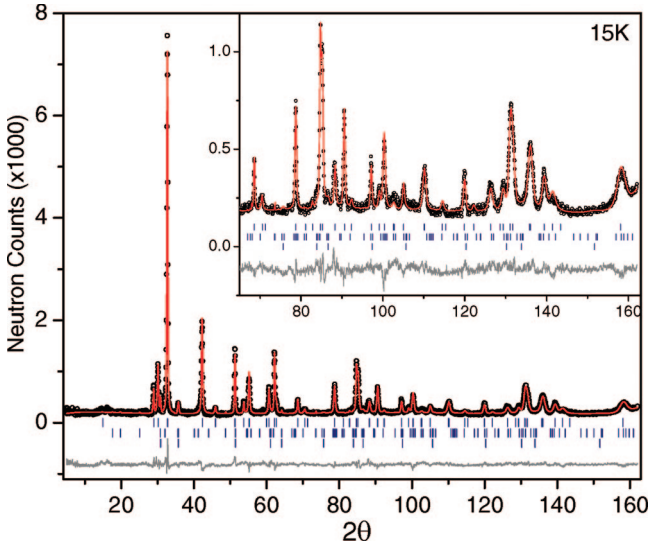

Figure 1. Experimental (circles), calculated (line), and difference (line below observed and calculated patterns) NPD profiles for $Li_2Ca(ND)_2$ at 15 K. The patterns also contain peaks from small amounts of $LiND_2$ (1.09 wt %) and CaND (2.98 wt %). Vertical bars indicate the calculated positions of Bragg peaks for $Li_2Ca(ND)_2$, $LiND_2$, and CaND (from the top), respectively. λ = 1.5403 Å.

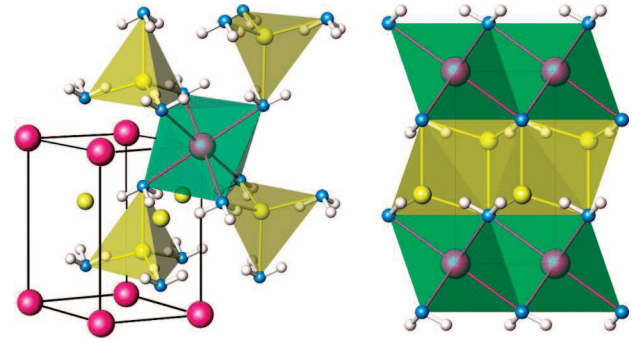

Figure 2. (Left) Off-[110] view of the refined trigonal structure of $Li_2Ca(NH)_2$. $Ca(NH)_6$ octahedra are in green; $Li(NH)_4$ tetrahedra are in yellow. Ca, Li, and N atoms are represented by large pink, yellow, and blue spheres, respectively. H atoms are randomly distributed at one of the three white sites around each N atom. (Right) Layered structure of $Li_2Ca(NH)_2$ viewed as a "combined imide" consisting of ordered CaNH layer and Li_2NH layer.

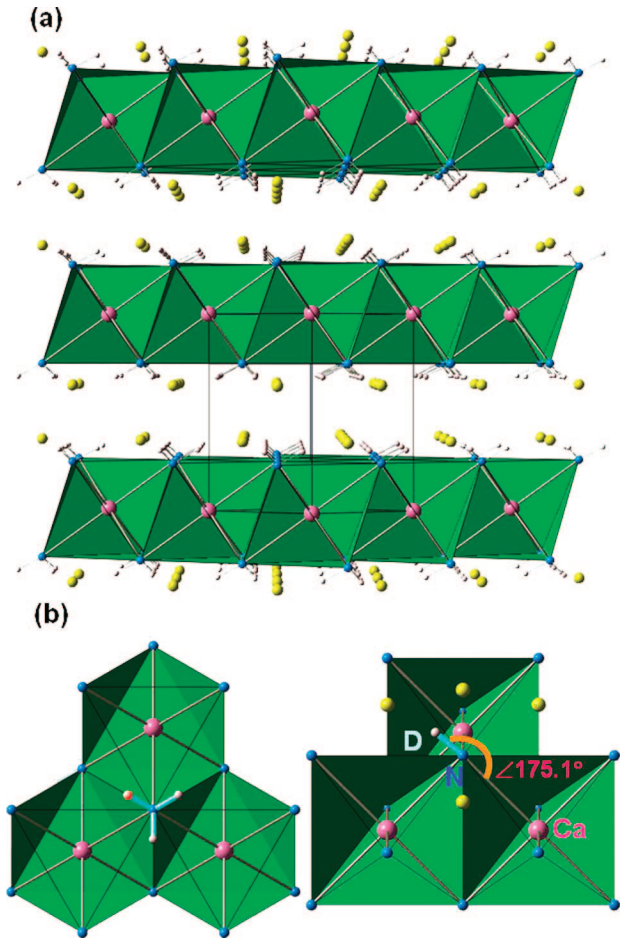

Figure 3. (a) Structure of $Li_2Ca(NH)_2$ viewed as a "intercalated" layered structure consisting of 2D slabs of $Ca(NH)_6$ octahedra separated by Li ion motifs. Ca, Li, N, and H atoms are colored as in Figure 2. (b) Left: 6*i*-model with D distributed at one (highlighted in red) of the three white positions around each N. Right: Refined 6*i*-model structure where N−D imide group is aligned along the Ca−N bond with ∠Ca−N−D = 175.1° (only show one D site for clarity).

distribute in one of three sites around each N, no matter which site H occupies, the resulting N−H bond is aligned along the corresponding Ca−N bond with H pointing opposite to Ca (see Figure 3b). Such a bonding orientation can be rationalized via the bonding between these ions. In imides, H and N are known to be covalently bonded via sharing of two valence electrons. Strictly speaking, the bonding should be polar-covalent where N has a greater portion of the valence electron density than H, which is thus somewhat positively charged. Nitrogen in the imide group still needs two more electrons to meet the eight-electron rule. Calcium donates its two valence electrons completely to the NH^{2-}, becoming Ca^{2+}. Therefore, the electrostatic repulsion between Ca^{2+} and H will drive them away from each other to reduce the overall energy. Our results suggest that the most stable arrangement with the lowest energy is a configuration with H−N−Ca bonding arrangement. In the refined structure, the D−N−Ca bond angle is ∼175.1°, very close to a linear line. Therefore, the electrostatic repulsion between H and the strong electropositive cation is apparently the primary factor responsible for the orientation of N−H bonds and the H positions. Of course, at any time the hydrogen is aligned along one N−Ca bond to maintain the minimum repulsion from this Ca^{2+}. But it also receives more repulsion from the other two adjacent Ca^{2+} cations, which tends to push the hydrogen to another site with the largest separation from another Ca^{2+}. Consequently, the NH^{2-} anion is not fixed with a certain "ordered" N−H orientation but rather rotating between the three possible sites around the N center. This effect is also consistent with the observations in other imides. For example, in $Li_2Mg(NH)_2$ the protons in imide groups are always associated with the neighboring cation vacancies, so as to maintain a minimized repulsion from the cations. Such an arrangement is found in the ordered structure of Li_2NH as well. In $Li_2Ca(NH)_2$, NH^{2-} are also bonded with Li^+, which may have some impact on the N−H orientation. The repulsion from the Li^+ on top of the NH^{2-} and from the Li^+ which the N−H orients toward tends to push the N−H away from the ideal 180° Ca−N−D angle. However, compared to Ca^{2+}, the smaller ionic radius, lesser ionic character, and smaller charge of Li^+ make its bonding strength with NH^{2-} much weaker. As a result, the effect of Li^+ on the N−H orientation is secondary, and thus there is only a small deviation from the ideal 180° for the Ca−N−H bond angle. Finally, we should note that attempts to fit our NPD data with other models with different D sites all resulted in the poor quality of fit and abnormal N−D distances; this is further evidence for the primary effect of the more electropositive Ca^{2+} on the orientations of N−D.

From the discussion above, it is clear that binary alkali or alkaline earth imides and their analogous oxides commonly show similar structures due to the equivalent charges of NH^{2-} and O^{2-}. It would thus be interesting to classify the structure of ternary imides into two categories: (i) For cations with similar sizes and coordination preferences, the resulting $A^+_nB^{2+}_m[NH]_{(n+2m)/2}$ may be isostructural with the parent imide (or its oxide analogue) with a formula written as $[A^+_{2n/(n+2m)}B^{2+}_{2m/(n+2m)}\square_{2m/(n+2m)}][NH]$ (i.e., $Li_2Mg(NH)_2$); (ii) For cations with significant size and coordination differences, the resulting ternary will form a combined imide consisting of A_2NH and BNH imide layers with a formula written as $A_{2n}B_m(NH)_{n+m}$ (i.e., $Li_2Ca(NH)_2$). In either case, compared to pure Li_2NH, the ternary imide is expected to exhibit faster Li^+ mobility, thanks to the presence of cation vacancies or open 2D channels for smaller mobile species defined by the layers of larger cation polyhedra. Such structure characteristics could have a great impact on hydrogen storage properties, as discussed below.

3.2. Hydrogenation/Dehydrogenation Mechanism. To understand the formation of the $Li_2Ca(NH)_2$ ternary compound, intermediate products at different dehydrogenation stages of the $2LiNH_2 + CaH_2$ mixture were monitored using X-ray diffraction (Figure 4). The XRD pattern on samples near the end of the heating ramp (1 °C/min) to 300 °C shows a multiphase mixture, including CaNH, Li_2NH, CaH_2, and $LiNH_2$ (Figure 4a). After staying at 300 °C for 30 min, CaNH, Li_2NH, and $LiNH_2$ remain, with the continued presence of $Li_2Ca(NH)_2$ and the absence of CaH_2 (Figure 4b). After complete dehydriding at 300 °C, the XRD pattern is dominated by $Li_2Ca(NH)_2$ (Figure 4c). When this product was rehydrogenated, 2H was absorbed, resulting in a mixture of CaNH, $LiNH_2$, and LiH (Figure 4d), different from the initial mixture $2LiNH_2 + CaH_2$. The H content in the rehydrogenated product was determined as Li/Ca/H = 2.02:1:4.01 by a PGAA technique. The refined NPD pattern, which contains a mixture of CaND + $LiND_2$ + LiD, collected on a deuterided sample after rehydrogenation can be found in the SI (Figure S5). Complete desorption of this rehydrogenated mixture produces $Li_2Ca(NH)_2$ with the same XRD pattern as that in Figure 4c.

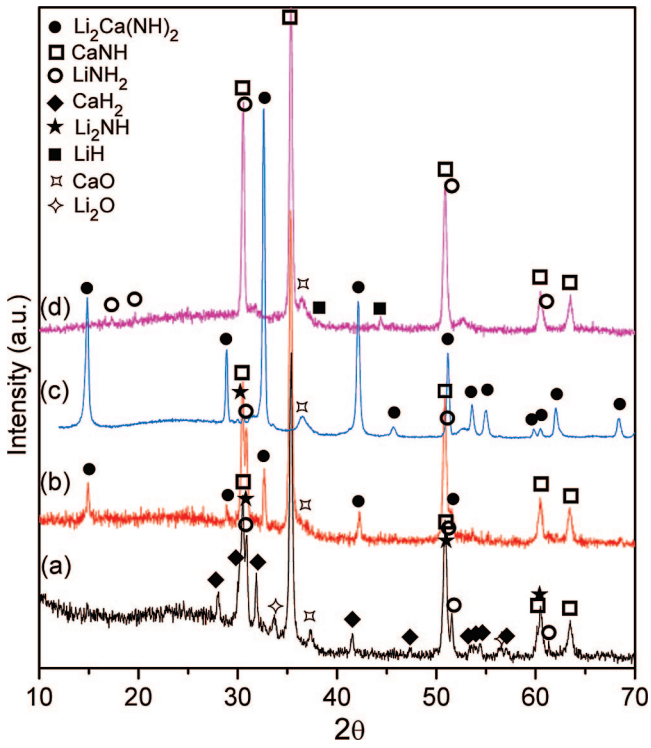

Figure 4. XRD patterns of products at various dehydrogenation/hydrogenation stages of $2LiNH_2 + CaH_2$. (a) Desorption during heating ramp to 300 °C, products: CaNH, Li_2NH, $LiNH_2$, and CaH_2; (b) desorption at 300 °C for 30 min, products: CaNH, Li_2NH, $Li_2Ca(NH)_2$, and small amount of $LiNH_2$; (c) desorption at 300 °C for 5 h, product: $Li_2Ca(NH)_2$; (d) hydrogenation of $Li_2Ca(NH)_2$ at 200 °C, products: $LiNH_2$, LiH, and CaNH.

In prior reports on the Li−Ca−N−H system, the mechanism of desorption from $LiNH_2$ and CaH_2 was suggested to be the direct reaction between amide and hydride.[9] This mechanism would require that $Li_2Ca(NH)_2$ be formed from the beginning of the dehydrogenation with the consumption of precursors $LiNH_2$ and CaH_2. However, our analysis at the initial decomposition step did not detect $Li_2Ca(NH)_2$ but CaNH and Li_2NH. And $Li_2Ca(NH)_2$ only appears after the formation of CaNH and Li_2NH.

In seeking an explanation for this complicated dehydrogenation and formation of $Li_2Ca(NH)_2$, it is useful to consider the structures of both precursors in the system. The previous study in $LiNH_2$ indicated the presence of Frenkel defect pair and the resulting motion of Li^+ and H^+.[2] We believe such movement of Li^+ and H^+ is still the key step. Furthermore, CaH_2 with an anti-$PbCl_2$ structure is known as an electrolyte material with highly mobile H^- ions.[18,19] Structural studies in CaH_2 also indicate the presence of a small amount of hydrogen vacancies and high H diffusion rates between the lattice sites at elevated temperatures.[20,21] Indeed, a recent study in the Li−Ca−N−H system revealed that the mixture of $2LiNH_2 + CaH_2$ shows a much faster dehydrogenating reaction and lower hydrogen T_{des} than those by starting from $Ca(NH_2)_2 + 2LiH$.[10] Therefore, not only Li^+ and H^+ in $LiNH_2$ but also H^- in CaH_2 will be involved in the ionic mobility and the dehydrogenation/hydrogenation mechanism of the mixed amide and hydride system at high temperature. Below, we will discuss the processes of dehydrogenation of the $2LiNH_2 + CaH_2$ mixture, hydrogenation of $Li_2Ca(NH)_2$, and desorption of the rehydrogenated product, which we believe best explain our structure results and the chemistry of the system.

3.2.1. Dehydrogenation of 2LiNH + CaH_2. In $LiNH_2$ the formation of a short-lived Frenkel defect pair first creates two adjacent, charged interstitial $[Li_iLiNH_2]^+$ and a tetrahedral lithium vacancy $[\square_{Li}NH_2]^-$, where "Li_i" with subscript "i" represents interstitial Li and "$\square_{Li}$" with subscript "Li" is the Li vacancy (eq 1 in Scheme 1). As proposed previously,[2] besides the recombination of the Frenkel-defect pair, the charge balance may also be restored by a subsequent motion of a Li^+ (eq 2 in Scheme 1) or a proton (eq 3 in Scheme 1) from $[Li_iLiNH_2]^+$.

In addition, hopping of a H^- ion in CaH_2 will also create a Frenkel defect pair, which produces two adjacent charged species, anion interstitial $[CaH_2H_i]^-$ and vacancy $[CaH\square_H]^+$, where "H_i" with subscript "i" represents interstitial H and "$\square_H$" with subscript "H" is the H vacancy (eq 4 in Scheme 1). These two unstable species could certainly be restored by the movement of H^- back to its original site, but the charge balance could also be maintained by a subsequent hopping of a H^- (eq 5 in Scheme 1). The highly mobile, free H^- anion in CaH_2 and protonic H^+ in $LiNH_2$ can very easily combine to create H_2 gas thanks to a very high enthalpy of the reaction (eq 6 in Scheme 1, $H^+ + H^- \rightarrow H_2 + \Delta H$, $\Delta H = -17.37$ eV).

The fast combination of H^+ and H^- leaves $[\square_{Li}NH_2]^-$ and $[CaH\square_H]^+$ in $LiNH_2$ and CaH_2, respectively, and drives the reaction between these two defects on the surface of adjacent $LiNH_2$ and CaH_2 particles (eq 7 in Scheme 1, i.e., $[\square_{Li}NH^{+\delta}{}_2]^- + [CaH^{-\delta}\square_H]^+ \rightarrow CaNH + H_2$). Our materials are mixed via mechanical ball-milling so that $LiNH_2$ and CaH_2 are in homogeneous contact, with particle sizes in the micrometer regime. The positively charged H^+ in the amide group and the H^- anion in CaH_2 will also combine to form H_2 during this defect reaction. When these processes occur, a mixture of $2LiNH_2 + CaH_2$ will release $2H_2$ in total, consistent with the hydrogen amount observed. Indeed, the prior desorption study of $2LiNH_2 + CaH_2$ indicated that H_2 started to release at as low as 50 °C, and two hydrogen desorption peaks were observed at 140 and 206 °C.[14]

Of course, a small amount of intermediate ammonia may also be formed by the proposed reaction[2] (eq 2),

$$[_{Li}NH_2]^- + H^+ \rightarrow NH_3 \qquad (2)$$

but consistent with previous studies,[10,14] ammonia was undetectable by MS during desorption, indicating that the amount of ammonia released was negligible in the present system. Therefore, the ammonia adduct in this mechanism must subsequently react in a very short time scale with the surface of nearby calcium hydride and form $Ca(NH_2)_2$ (eq 3a). The resulting $Ca(NH_2)_2$ continues to react with CaH_2 and produces CaNH by eq 3b.

$$NH_3 + 1/2CaH_2 \rightarrow 1/2Ca(NH_2)_2 + H_2 \qquad (3a)$$

$$1/2Ca(NH_2)_2 + 1/2CaH_2 \rightarrow CaNH + H_2 \qquad (3b)$$

However, the desorption study of $Ca(NH_2)_2$ indicated that $Ca(NH_2)_2$ desorbs NH_3 more easily than $LiNH_2$, and the

(18) Zhu, B. *J. Mater. Sci. Lett* **1999**, *18*, 1807–1809.
(19) Zhu, B.; Liu, X. *Electrochem. Commun.* **2000**, *2* (1), 10–14.
(20) Anderson, A. F.; Maeland, A. J.; Slotfeldt-Ellingsen, D. *J. Solid State Chem.* **1977**, *20*, 93–101.
(21) Wu, H.; Zhou, W.; Udovic, T. J.; Rush, J. J.; Yildirim, T. *J. Alloys Compd.* **2007**, *436*, 51–55.

Scheme 1. Dehydrogenation of 2 $LiNH_2$ + CaH_2 with $2H_2$ Totally Released and Products of CaNH, Li_2NH, and/or $Li_2Ca(NH)_2$ Observed at Various Desorption Steps

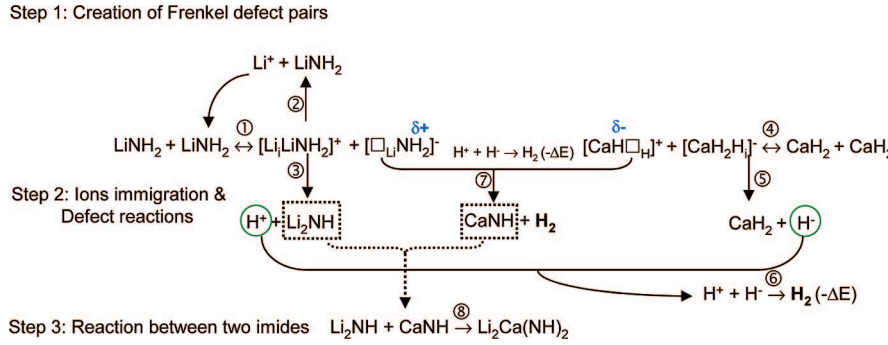

Scheme 2. Hydrogenation of $Li_2Ca(NH)_2$ with 1 H_2 Totally Absorbed and Final Products of CaNH, $LiNH_2$, and LiH

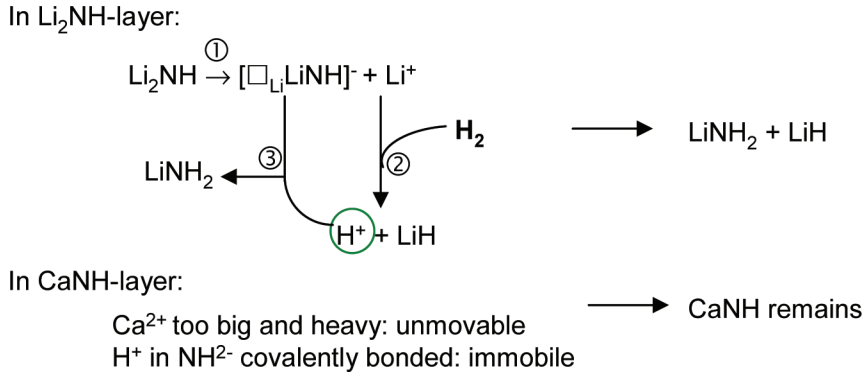

desorption of NH_3 occurs before H_2 is released.[22] We did not detect the formation of $Ca(NH_2)_2$ in the XRD pattern of initial desorption products or a NH_3 release. Therefore, the reaction of H^- and H^+ must dominate and consume most of the protonic H, rather than reaction 2. As a result, we observed the formation of Li_2NH, CaNH, as well as the unreacted $LiNH_2$ and CaH_2, at the initial stage of desorption. Although our materials are mixed evenly in small particles, we believe the ionic mobility mechanism rather than the direct reaction[9] is still the most likely mechanism. With further release of H_2, all CaH_2 converted to CaNH, which reacts with Li_2NH to form $Li_2Ca(NH)_2$, as in a normal solid state reaction. Scheme 1 illustrates all the possible reactions involved in the dehydrogenation of $2LiNH_2$ + CaH_2. Of course, the processing of the ternary, i.e., mixing, origin, and purity of the raw materials, can have a profound effect on the reactivity and purity of the final products. In the present study, hydrogenated ternary was prepared using mechanical milling of commercial lithium amide and calcium hydride, while deuterated ternary was prepared using hand-grinding with a pestle and mortar from laboratory-made deuterated lithium amide and calcium deuteride. As a result, we see a nearly single-phase ternary in the former case (a small amount of Li_2O associated with the impure starting materials was also observed; see SI), along with a small amount of unreacted CaND and $LiND_2$ in the latter (see Figure 1).

3.2.2. Hydrogenation of $Li_2Ca(NH)_2$. As we mentioned above, the structure of $Li_2Ca(NH)_2$ can actually be viewed as a combined structure with alternating Li_2NH and CaNH layers. The hydrogenation process will then occur within these imide layers, separately. In the layer of Li_2NH, mobile Li produces Li^+ interstitials and Li vacancies ($[\square_{Li}LiNH]^-$). The Li^+ reacts rapidly with hydrogen gas, forming LiH and a proton (eq 2 in Scheme 2). The proton produced will then react with the negatively charged Li-vacancy and bond with the imide group to form an amide group (eq 3 in Scheme 2). These processes are similar to those in Li_2NH but occur only in two dimensions within $LiNH_2$ layers.

While in the layers of CaNH there is no mobile species; i.e., protons in NH^- groups are covalently bonded, and Ca^{2+} cations are too heavy and large to migrate. Consequently, the "inert" CaNH remains. Continuous ion movement and interactions in the Li_2NH layer will finally dissociate $Li_2Ca(NH)_2$ into $LiNH_2$, LiH, and unreacted CaNH, as observed in our XRD results. Therefore, two H's will be absorbed by one $Li_2Ca(NH)_2$ formula unit (eq 4),

$$Li_2Ca(NH)_2 + H_2 \rightarrow LiNH_2 + LiH + CaNH \qquad (4)$$

and the final hydrogen to metal ratio is Li/Ca/H $\approx$ 2:1:4, consistent with the PGAA results. The formation of these products was also confirmed by the refinement on the NPD data collected from a sample after deuteriding $Li_2Ca(ND)_2$ (see Figure S5 in the SI). The distinctive reflections at d = 5.117, 4.521, 3.561, 2.520, etc. in the NPD pattern indicate the presence of $LiND_2$ ($I\bar{4}$)[17] and the absence of $Ca(ND_2)_2$ ($I41/amd$),[1] supporting the rehydrogenation mechanism presented here, and clarifying the previously claimed products of $Ca(NH_2)_2$ and LiH after rehydrogenation.[10] Scheme 2 shows all the reactions on hydrogenating $Li_2Ca(NH)_2$.

(22) Hino, S.; Ichikawa, T.; Leng, H.; Fujii, H. *J. Alloys Compd.* **2005**, *398*, 62–66.
(23) Senker, J.; Muller, M.; Press, W.; Muller, P.; Mayer, H. M.; Ibberson, R. M. *J. Phys. Chem. B* **1998**, *102*, 931–940.
(24) Yang, J.; Sudik, A.; Siegel, D. J.; Halliday, D.; Drews, A.; Carter, R. O., III; Wolverton, C.; Lewis, G. J.; Sachtler, J. W. A.; Low, J. J.; Faheem, S. A.; Lesch, D. A.; Ozolins, V. *Angew. Chem., Int. Ed.* **2008**, *47*, 882–887.

Table 2. Selected Interatomic Distances (Å) and Bond angles (deg) in $Li_2Ca(ND)_2$ (6*i*-Model)

	5 K	295 K
	atom 1−atom 2	
Ca−N (6×)	2.527(2)	2.539(2)
Ca−D	2.621(5)	2.623(4)
Li−N (1×)	2.291(4)	2.305(9)
Li−N (3×)	2.167(3)	2.167(3)
Li−D (3×)	1.363(5)	1.364(8)
Li−D (3×)	1.998(1)	2.024(1)
Li−Li (3×)	2.606(1)	2.627(1)
N−D (3×)	0.835(5)	0.832(8)
	bond angle	
N−Ca−N	89.50(1)	89.27(1)
N−Ca−N	90.50(1)	90.73(1)
N−Ca−N	180	180
N−Li−N	110.4(2)	110.7(2)
N−Li−N	108.5(2)	108.1(2)
Ca−N−D	175.1(4)	174.0(5)
Li−N−D	12.3(3)	11.6(4)
Li−D−N	160.3(3)	161.3(7)

Scheme 3. Dehydrogenation of CaNH + $LiNH_2$ + LiH Mixture (i.e., the Hydrogenated Products from $Li_2Ca(NH)_2$) with 1 H_2 Totally Released and Final Products of $Li_2Ca(NH)_2$

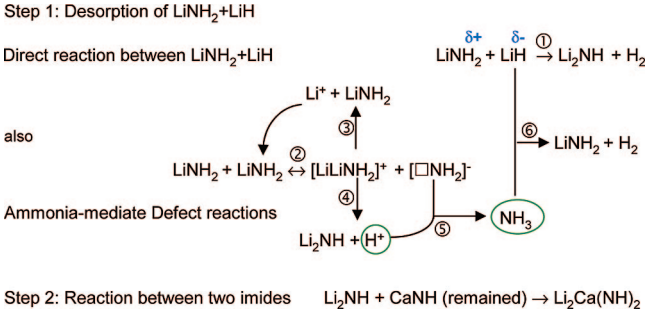

From this work and a prior absorption study,[9] $Li_2Ca(NH)_2$ could absorb H_2 at temperatures ~130 °C lower than that of Li_2NH. Considering the structural characteristics of the ternary imide, i.e., Li^+ ions are "intercalated" between 2D layers of $Ca[NH]_6$ octahedra, we believe the rapid Li motion within these 2D channels will have a significant impact on the hydrogenation process. The facile mobility of Li within the 2D channels is also confirmed by the observed increasing nonstoichiometry at Li lattice sites with elevated temperature (see Table 2). Therefore, it is such a special layered structure with "intercalated" Li ions that is mainly responsible for the dramatically lowered T_{abs}.

3.2.3. Desorption of Hydrogenated $Li_2Ca(NH)_2$. For the dehydrogenation of the mixture of $LiNH_2$, LiH, and CaNH, Li_2NH can be formed by the direct reactions between amide and hydride due to the close proximity of particles (eq 1 in Scheme 3). The formation of a small amount of ammonia is also possible (eq 5 in Scheme 3), but the NH_3 molecules produced will react rapidly with the surface of adjacent LiH and release H_2. The dehydrogenated product Li_2NH then reacts with the remaining CaNH and forms $Li_2Ca(NH)_2$. All the reactions are shown in Scheme 3.

In summary, the movement of Li^+ and H^+ has been shown to be the key process involved in both decomposition and hydrogenation of $LiNH_2/Li_2NH$ and the production of ammonia. In the case of mixed amide and hydride, we found not only the migration of Li^+ and H^+ but also mobile H^- in hydrides play a key role in dehydrogenation and hydrogenation. The major benefit of the participation of H^- is the enhanced interaction between H^- and H^+ that promotes hydrogen to be released at lower temperature and reduction in the interaction between H^+ and NH^{2-} to produce ammonia. This process also drives the subsequent interactions between the other positively and negatively charged species. Moreover, the resultant ternary imide with a layered structure allows rapid Li^+ ionic movement, leading to a much lower T_{abs} compared to Li_2NH. Therefore, we conclude that the differently charged small mobile species are primarily responsible for the reduced T_{des}/T_{abs} and for the minimized ammonia release in the mixed amide/hydride system.

Such a mechanism is also valid for the significantly decreased T_{abs} in ternary imide $Li_2Mg(NH)_2$. A mixture of $Mg(NH_2)_2$ + 2LiH was observed after hydrogenating $Li_2Mg(NH)_2$.[8,9] As noted earlier, $Li_2Mg(NH)_2$ forms a vacancy-containing structure derivative such as Li_2NH due to the similar size of Mg^{2+} and Li^+ and can be written as $(LiMg_{0.5}\square_{0.5})NH$. In such a structure, Li^+ ions migrate through the cation vacancies and interact with H_2 applied, forming LiH and H^+ (eqs 5 and 6). The proton produced will be attracted toward the negatively charged region, forming $Mg(NH_2)_2$, consequently (eq 7).

$$(LiMg_{0.5}\square_{0.5})NH \rightarrow [(\square_{Li}Mg_{0.5}\square_{0.5})NH]^- + Li^+ \quad (5)$$

$$Li^+ + H_2 \rightarrow LiH + H^+ \quad (6)$$

$$H^+ + [(\square_{Li}Mg_{0.5}\square_{0.5})NH]^- \rightarrow [(Mg_{0.5}\square_{0.5})NH_2] \quad (7)$$

Apparently, a large amount of cation vacancies plays an important role in facilitating the migration of small mobile Li^+ and H^+ and, therefore, is responsible for the reduced T_{abs} of $Li_2Mg(NH)_2$. In addition, the presence of cation vacancies could also enhance the reactivity of the ternary imide, which has been shown as "self-catalyzing" seed in improving the desorption kinetics of $Mg(NH_2)_2$ + 2LiH.[24]

Our results and discussion demonstrate that the mobility of small ions in the mixed amide/hydride system has a great impact on the hydrogen-storage properties. Thus any approach, such as introduction of vacancies or potential charge carriers, the formation of special crystal structures, and reduction of the diffusion distance through decreasing particle size, etc., that can facilitate the migration of small ions could dramatically benefit the absorption and desorption performance.

4. Summary

The structure of ternary imide $Li_2Ca(NH)_2$ was determined using NPD data on a deuterated sample. $Li_2Ca(NH)_2$ crystallized in a layered structure consisting of infinite 2D slabs of edge-shared $Ca[NH]_6$ octahedra separated by the motif of Li cations. From the detailed analysis of the various stages of desorption and absorption of the $2LiNH_2 + CaH_2$ mixture, we concluded that, compared to pure amide, the reduced T_{des} of the mixed amide and hydrides is due to the migration of H^- in the hydride. Comparison of the T_{abs}'s on the pure Li_2NH and ternary imides with special structural characteristics indicated that changes in the hydrogen-storage performance are dominated by the structural arrangements allowing the mobility of small ions.

Acknowledgment. I would like to thank Dr. John J. Rush and Dr. Wei Zhou for their valuable comments on this paper.

Supporting Information Available: Details of structure determination and refinement on various models with dif-

ferent D sites. Crystallographic information for the refined structures (6*i*-model), including crystallographic information files (CIF) for structures of $Li_2Ca(ND)_2$ at 15 K and 295K, NPD patterns of refined data of $Li_2Ca(ND)_2$ at 295 K, and NPD patterns of refined data of $Li_2Ca(NH)_2$ at 295 K. Refined crystallographic data of 12*f*-model. These materials are available for free of charge via the Internet at http://pubs.acs.org.

JA800300E